

Fully 3D-printed gripper jaw with embedded sensitive sensor structures for robotic applications

Nikolai Hangst, Thomas Wendt, Stefan Rupitsch

Zitiervorschlag im APA Stil:

Hangst, N., Wendt, T., & Rupitsch, S. (2026). Fully 3D-printed gripper jaw with embedded sensitive sensor structures for robotic applications. *Sensors and Actuators A: Physical*, 399, 1–12. <https://doi.org/10.1016/j.sna.2025.117334>

Abstract

In this contribution, we present a novel, fully 3D-printed sensitive gripper jaw for high gripping forces up to 40 N. The fabrication process is based on fused layer manufacturing, in which two different materials are sequentially extruded. The gripper jaw is based on a sensor design with multiple-stacked bending beams and four sensor elements, each printed directly into one of the upper and lower bending beams. The research focuses on the sensor design of the gripper jaw, the mathematical description and simulation, the fabrication process, the electrical characterization of the sensor material, and the sensitivity behavior of the gripper jaw in terms of zero-point deviation, characteristic value deviation, linearity behavior, repeatability, and viscoelastic behavior. In addition, the gripper jaw is compared with a similarly manufactured gripper jaw with conventionally attached strain gauges, as well as with other comparable fully 3D-printed sensors to classify the sensor quality. The results demonstrate that the fully 3D-printed gripper jaw is partially suitable for sensitive and fragile components. The gripper jaw is well suited for detecting the gripping state (part gripped / not gripped).

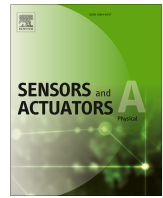
Nutzungsbedingungen

Dieses Dokument wird unter diesen Bedingungen zur Verfügung gestellt:
Creative Commons - CC BY - Namensnennung 4.0 International
Für weitere Informationen siehe:
<https://creativecommons.org/licenses/by/4.0/deed.de>



Kontakt

Hochschule Offenburg | Bibliothek
Badstraße 24
77652 Offenburg
Telefon: (0781) 205-240
E-Mail: bibliothek@hs-offenburg.de
www.hs-offenburg.de/bibliothek



Fully 3D-printed gripper jaw with embedded sensitive sensor structures for robotic applications

Nikolai Hangst^{a,*}, Thomas M. Wendt^a, Stefan J. Rupitsch^b

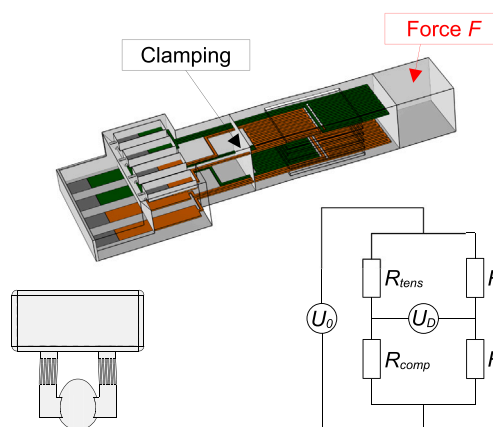
^a Work-Life Robotics Institute, Offenburg University of Applied Sciences, Max-Planck Straße 1, 77656 Offenburg, Germany

^b Laboratory for Electrical Instrumentation and Embedded Systems, Department of Microsystems Engineering, University of Freiburg, Georges-Köhler-Allee 106, 79110 Freiburg, Germany

HIGHLIGHTS

- Fully 3D-printed functional gripper jaw.
- Structural and sensing functions integrated in a single additive process.
- Simulation and analytical model are consistent with experimental results.
- Sensor shows a high gauge factor of 3.8 compared to conventional metals.
- High gripping force of 40 N achieved.

GRAPHICAL ABSTRACT



ARTICLE INFO

Keywords:

3D-printing
Fully 3D-printed force sensor
Robotic applications
Sensitive gripper
Sensitive gripper jaw

ABSTRACT

In this contribution, we present a novel, fully 3D-printed sensitive gripper jaw for high gripping forces up to 40 N. The fabrication process is based on fused layer manufacturing, in which two different materials are sequentially extruded. The gripper jaw is based on a sensor design with multiple-stacked bending beams and four sensor elements, each printed directly into one of the upper and lower bending beams. The research focuses on the sensor design of the gripper jaw, the mathematical description and simulation, the fabrication process, the electrical characterization of the sensor material, and the sensitivity behavior of the gripper jaw in terms of zero-point deviation, characteristic value deviation, linearity behavior, repeatability, and viscoelastic behavior. In addition, the gripper jaw is compared with a similarly manufactured gripper jaw with conventionally attached strain gauges, as well as with other comparable fully 3D-printed sensors to classify the sensor quality. The results demonstrate that the fully 3D-printed gripper jaw is partially suitable for sensitive and fragile components. The gripper jaw is well suited for detecting the gripping state (part gripped / not gripped).

* Corresponding author.

Email addresses: nikolai.hangst@hs-offenburg.de (N. Hangst), thomas.wendt@hs-offenburg.de (T.M. Wendt), stefan.rupitsch@imtek.uni-freiburg.de (S.J. Rupitsch).

<https://doi.org/10.1016/j.sna.2025.117334>

Received 28 July 2025; Received in revised form 3 November 2025; Accepted 25 November 2025

Available online 6 December 2025

0924-4247/© 2025 The Authors. Published by Elsevier B.V. This is an open access article under the CC BY license (<http://creativecommons.org/licenses/by/4.0/>).

1. Introduction

Ensuring safety in industrial and collaborative robotics is one of today's central issues. In this context, the robot and its peripherals, such as the gripper, must be considered [1,2]. This requires measuring and controlling the gripping force acting on the workpiece with appropriate sensors [3,4]. Commercial grippers typically estimate this force indirectly via motor current measurements in the drive train, as also confirmed by Saadatzi et al. [3]. In contrast, our approach enables the direct measurement of the force acting on the gripper jaws. Another aspect of sensitive gripping technology is the handling of sensitive and fragile components [3,4]. In this case, the adaptation of the gripper or the gripper jaws to the respective components by means of conventional manufacturing is a significant cost driver, which can be reduced by additive manufacturing [3,5,6].

1.1. Motivation

3D printing, a subset of additive manufacturing, has expanded significantly in materials and manufacturing processes since its inception in 1986 [7,8]. Over the past few years, it has increasingly been applied to the fabrication of robotic grippers and gripper jaws. Recent studies demonstrate the versatility of this technology, ranging from mechanically customized designs [2,5,9–12] and fiber-reinforced structures [13] to concepts with integrated sensing or actuator functionalities, including soft robotic approaches [6,14–22]. Recent developments include processing conductive materials to fabricate electrical circuits and components [7]. Three manufacturing processes are available: hybrid approach, conductor infusion, and multi-material printing. In the hybrid approach and conductor infusion, the printing process is interrupted to allow the integration of electronic components into a structural component or the application of ink, paste, or adhesive in a subsequent process. In contrast, multi-material printing does not interrupt the printing process because all materials (conductive and non-conductive) are processed in one process [23–26]. Another approach is to create a structural component with cavities filled with liquid metal paste [27].

A subset of 3D-printed electronics is 3D-printed sensors. In robotics, 3D-printed force or strain sensors have proven particularly useful in robot gripping systems due to their high sensitivity [27,28]. In many cases, strain gauge technology is used for force sensing, which is considered one of the most fundamental sensing devices [4,26,29]. The function of these sensors is based on the principle of resistance change during deformation. The piezoresistive behavior of the sensor element leads to a change in resistance caused by a change in the geometry of the conductor paths and a change in the specific resistance of the sensor material during deformation [4,25,28–31]. The sensitivity of the sensor elements is defined by the k -factor (gauge factor), relating the relative resistance change to the applied mechanical strain [4,28,31,32]. The strain gauge is typically evaluated with temperature-compensated half- or full-bridge circuits with a coupled low-cost evaluation unit [4,15,26,33]. The ability to fabricate strain gauges utilizing 3D printing allows for fast, inexpensive, and easily customizable force sensors and the possibility of placing strain gauges in locations within the components [26,33]. 3D-printed force sensors provide a low-cost alternative to conventional strain gauges [29]. In this context, additive manufacturing offers additional advantages. It allows single-step, fully automated fabrication [5–7,17,34], provides high design freedom to integrate structural and functional elements [6,7,26,27,34–36], and enables geometry adaptation for specific stiffness or shape requirements [2,5,6,17].

Conductive materials are essential for the fabrication of 3D-printed electronics and sensors [22,32,34]. These materials include conductive inks, pastes, adhesives, or conductive polymer composites [8,23]. Examples of inks include silver inks, nanosilver inks, and gold nanoparticle inks [7,26,27,33,37]. The advantage of nanoparticle inks is the lower curing temperature, which depends on the particle size. This ranges from 150 °C to 250 °C [26]. Conductive polymer composites consist of a polymer with a conductive filler [7,22,38]. Both elastic and rigid

materials are utilized as the base. Examples include PLA, ABS, PEEK, or TPU [22,23,33]. Fillers can be carbon nanotubes (CNT) in the form of single or multi-walled carbon nanotubes (SWCNT, MWCNT), carbon black, graphite, graphene, metal powder, or silver flakes [22,23,25–28,32,33,37,39]. Contact between the filler particles in the polymer matrix forms a conductive path through the polymer [24,32,38]. Conductive polymer-based materials are often applied to manufacture strain gauges [33]. The advantage compared to metals is the higher sensor sensitivity with a k -factor of more than 100,000. In addition, polymer composite sensors have a cycle life of up to 180,000 [28]. Conductive inks and pastes are an alternative, but they are more expensive and have a high melting point above 250 °C for curing [7,26]. In addition, they cannot be processed on a non-customized 3D printer [8]. The disadvantage of conductive polymer composites is their high resistivity.

Conductive polymer composites are typically processed by fused layer manufacturing (FLM). A significant advantage of this method is the ability to combine different materials including conductive polymer composites in a single process [22–24]. This allows electrical circuits and components to be integrated directly into the 3D-printed structure [24], enabling the fabrication of robotic grippers and gripper jaws with integrated sensors [6,14,15,19,21,22]. Using this method, the sensor elements can be placed inside the 3D-printed components, which is not possible with conventional manufacturing methods [26]. Alternative methods for fabricating 3D-printed sensors include stereolithography, direct light processing or projection stereolithography, polyjet, and aerosol jet [26,29].

1.2. Contribution

This contribution proposes a sensitive gripper jaw with the properties of a multiple-bending-beam structure and embedded piezoresistive sensor elements made of a polymer composite material with an extended gripping force range of 0 N up to 40 N. The design is based on Hangst et al. [18], with the difference that this sensor is entirely fabricated using 3D printing. An analytical and numerical model approach are presented to describe the sensitive behavior of the gripper jaw. Missing material properties for the model adaptation are determined based on measurement results. The work focuses on a detailed description of the fabrication of the sensitive gripper jaw and its characterization based on experimental investigations, including a discussion of the results.

2. State of the art

There have been many reports in scientific journals and conference proceedings on fabricating 3D-printed force sensors. These papers include both partially and fully 3D-printed sensors made of polymer composites. The following overview focuses exclusively on resistive, strain-gauge-based force sensors embedded in structural components fabricated using the FLM process, excluding sensors integrated into soft robotic grippers and highly flexible designs.

One of the most essential partially 3D-printed force sensors for micro-scale applications is the strain gauge micro force sensor presented by Qu et al. [35,36] to determine Young's modulus of polydimethylsiloxane samples with different cross-linking degrees. The spring body of the load cell was fabricated on a Prusa i3 3D printer using PLA as the print material. The sensor has a sensitivity of 1.369 V/V/N and a linearity deviation of 1.14 % with a measuring range of 0 N to 0.18 N. Another example is a three-axis micro force sensor measuring contact force on freely moving *Drosophila* larvae by Pan et al. [40]. The sensor was fabricated on an Ultimaker 2 using TPU as the substrate. The sensor has a measurement range of 0 N to 0.012 N in all three axes, a sensitivity between 22.42 V/N and 74.80 V/N, and a linearity deviation of less than 2 %. The bridge voltage is not specified. A sensor for higher gripping forces was presented by Hangst et al. [18], featuring a sensitive gripper jaw for robot grippers. Using a multiple-bending-beam structure, an increased measuring range of 0 N up to 40 N at a defined deflection of

the gripper jaw was achieved to reduce contact impacts during the gripping process. The spring body or measurement body was manufactured utilizing PETG on a Prusa MK3S printer. The sensor has a sensitivity of 0.148 mV/V/N and a linearity deviation of 0.14 %. The strain gauges were manually applied and connected to a Wheatstone full-bridge circuit.

The polymer strain gauge by Chadda et al. [29] and the fully 3D-printed force sensor by Herbst et al. [15] are among the most essential fully 3D-printed force sensors. Chadda et al. [29] demonstrated a sensor in which a conductive material was printed on a non-conductive substrate and glued to a stainless-steel body with superglue to function as a force sensor. The strain gauge was fabricated on a Prusa MK3S printer using conductive PLA as the sensor material and non-conductive PLA as the carrier material. The sensor was designed for a maximum force of 30 N in combination with the stainless-steel body and showed a sensitivity of 2.18 Ω /N, a linearity deviation of +3 %, -4 %, and a k -factor of 8.3. The strain gauge was evaluated via a digital multimeter instead of a measuring bridge. Building on this concept, Herbst et al. [15] extended it by fabricating the entire sensor, including the printed spring body. The sensor was designed for a maximum force of 20 N with a linearity deviation of 3.6 % and was evaluated using a half-bridge circuit. It was fabricated on a Raise3D printer using conductive PLA as the sensing material and non-conductive PLA as the carrier material. The sensor concept was later integrated into gripper jaws, demonstrating the potential of fully 3D-printed sensitive gripper jaws to detect object grasping. Another example are two low-cost load cells with four strain gauges by Andria et al. [26] and Stano et al. [33]. In this case, conductive PLA was used as the sensor material and TPU as the support material. The load cells were fabricated in a fully automated process on an Ultimaker 3 dual extruder. The fabrication time was about two hours, and the production cost was less than three Euros. The evaluation was performed with maximum sensitivity and temperature compensation using a full-bridge circuit. The measuring range of the sensors is 0 kg to 0.1 kg with a sensitivity of 88 mV/V/kg. The linearity deviation is not specified. Analogous to the partially 3D-printed sensor by Pan et al. [40], Kim et al. [24] present a fully printed multi-axis force sensor. The sensor is made of TPU and a TPU/CNT nanocomposite material and has a resistance per sensor element in the two- to three-digit kilohm range. It was manufactured using a Makerbot 2X Replicator 3D printer with dual print heads. The sensor has a measuring range of 0 N to 4 N, and neither sensitivity nor linearity have been specified. The different sensitivity and measuring ranges of all the sensors depend on the stiffness of their spring bodies and the piezoresistive properties of their sensing materials.

All fully 3D-printed force sensors show significantly higher inaccuracies compared to partially 3D-printed sensors. It can be concluded from the state of the art that all 3D-printed force sensors (partially and fully 3D-printed) are currently only designed for small force ranges up to the single-digit Newton range. Exceptions are the partially 3D-printed sensitive gripper jaw by Hangst et al. [18], the 3D-printed polymer strain gauge by Chadda et al. [29], and the fully 3D-printed sensor by Herbst et al. [15]. In Hangst et al. [18], higher forces are possible due to a special multiple-bending-beam structure. In Chadda et al. [29], the stainless-steel plate mainly picked up the force. In Herbst et al. [15], higher measurable forces result from a stiff beam design that causes asynchronous deformation. The reason for the primarily small measuring ranges is the lower load capacity compared to metals [8]. Except for Hangst et al. [18] and Herbst et al. [15], the force sensors described in the literature are not integrated into robot gripper jaws, although they are based on the same functional principle. In sensitive gripper jaws, we found that most sensors belong to the field of soft robotics [6,14,16,21–23].02. In this case, the focus is more on detecting the gripper fingers' positions to determine whether an object is grasped or not, rather than measuring the applied force.

3. Materials and methods

In this section, we present the materials and machines used, the material selection, the gripper jaw design, the analytical and simulation approaches for the mechanical and electrical sensor behavior, the 3D-printing fabrication process and sensor element interconnection, the measurement setup, and the arrangements for the measurements of the fully 3D-printed sensitive gripper jaw.

3.1. Materials and machines

We used polyethylene terephthalate glycol (Prusament PETG Signal White, Prusa Research) as the base material for the gripper jaw. Polylactide with carbon black filler (ProtoPasta PLA-C, Protoplant) was utilized as the conductive sensor material or polymer composite. The gripper jaw was fabricated on a 3D printer using the FLM process (Prusa MK3S, nozzle diameter 0.4 mm). The material change was performed manually through several print interruptions. Constantan wire, solder, self-adhesive copper foils, silver ink, and epoxy adhesive were used to connect the sensor elements to the measuring bridge on a circuit board.

3.2. Material selection

PETG is a good printable, semi-crystalline engineering material. The advantages include good mechanical properties up to a glass transition temperature of 80 °C, low creep, low humidity permeability, and resistance to chemicals and humidity. PLA has mechanical properties similar to PETG at room temperature. The disadvantages are a low glass transition temperature between 45 °C and 65 °C and embrittlement under UV radiation [38].

Based on the advantages mentioned above, PETG is the base material of the gripper jaw. The PLA-C from Protopasta used by Chadda et al. [29] was chosen for the conductive material, considering its good sensor properties with a linearity deviation of about +3 % to -4 % at a k -factor of 8.3. The combination of both materials is possible due to similar printing temperatures. The disadvantage of PLA regarding embrittlement due to UV radiation can be eliminated by embedding the material into the component. The glass transition temperature of 45 °C to 65 °C is also sufficient since gripper systems are usually used at room temperature. Even at higher temperatures, the surrounding PETG acts as a mold support and insulator, protecting the PLA.

3.3. Gripper jaw design

The gripper jaw design was adapted from Hangst et al. [18] and is based on a conventional single-point load cell with two bending beams (see Fig. 1a). This design was extended with several-stacked bending beams to form a multiple-bending-beam structure (see Fig. 1(b), enabling an almost parallel gripping of components with a flexible customization of the force-bending ratio. This ratio can be adjusted for specific applications by varying the number of bending beams and their thickness. The advantage of large deflections of the gripper jaw is that contact shocks are reduced by a delayed increase in force, improving the response time of downstream systems. Another advantage of the multiple-bending-beam structure compared to a double-bending-beam structure is the lower maximum mechanical stress in the component at the same deflection. This allowed conventional strain gauges to be applied at large deflections.

The significant difference compared to the partially 3D-printed sensitive gripper jaw designed by Hangst et al. [18] is the extension to a fully 3D-printed sensitive gripper jaw. The complete gripper jaw is fabricated in a single process using this approach. In addition, the sensor elements are embedded directly into the gripper jaw. The arrangement of the sensor elements is based on the literature [18,26,33,35,36]. The sensor elements were embedded in the second lowest and second highest beam for a better connection of the individual sensor elements in a 3D-printed circuit board housing at the front end of the gripper jaw (see

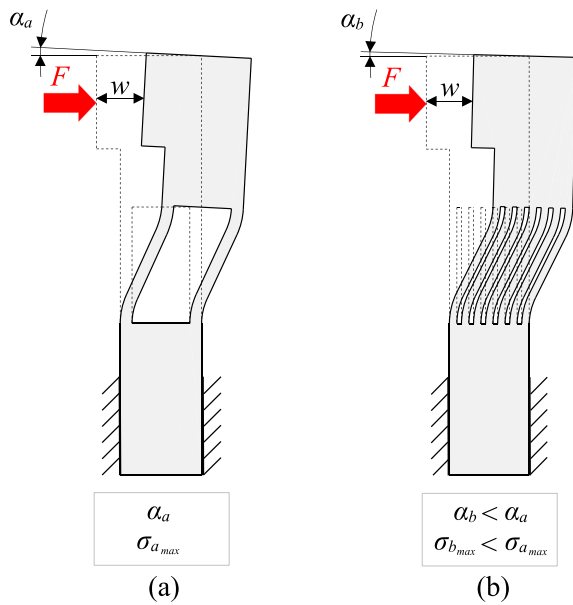


Fig. 1. Schematic representation of different gripper jaw structures. (a) Double-bending-beam structure, (b) multiple-bending-beam structure.

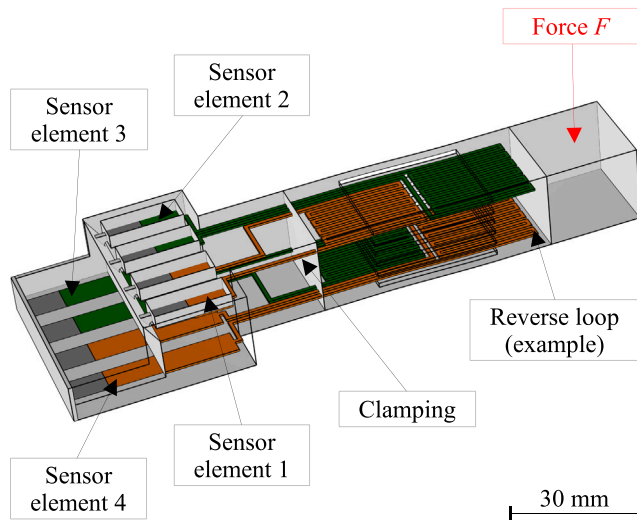


Fig. 2. Gripper jaw design with seven bending beams and four sensor elements.

Section 3.6.1). The sensor elements are each located one layer (0.2 mm) below or above the closest surface to protect them from environmental influences.

Fig. 2 shows the gripper jaw with sensor elements 1–4 and the corresponding force application and clamping. The gripping surface is customizable and has been omitted to simplify the illustration. The overall geometric dimensions of the sensor are 127 mm × 40 mm × 17.2 mm (length, width, depth) with the circuit board housing and 90 mm × 20 mm × 17.2 mm (length, width, depth) without the circuit board housing. The individual beams in the center of the jaw are 26 mm long with a beam thickness of 1.6 mm. The spacing between the beams is 1 mm. The measuring grids of the polymer composite sensor elements are arranged in a meandering pattern with a length of 20 mm and extend beyond the regions of significant bending stress along the beams. On one side, they end shortly before the points where bending stress reverses, and on the other side, they extend onto the solid part of the gripper jaw. This is

to improve the adhesion of the conductor tracks by increasing the contact area. Previous tests have shown that different material pairings can partially separate under load. In addition, the reverse loops have been placed far from any stresses to optimize force transfer and eliminate a predetermined breaking point transverse to the load direction. This also ensures good force introduction into the tracks by increasing and decreasing the load per track. A final benefit is the print quality before and after the reversal loops due to the reorientation of the print head. This results in a conductor track that is as homogeneous as possible in the force range.

The arrangement and structure of the sensor elements can be optimized to match the magnitude of the output signal for future work. This is not necessary for verifying the sensor behavior. The dimensions of the sensor elements extend over the entire width of the base body with a conductor track cross-section of 0.8 mm × 0.4 mm (width, depth) each. This corresponds to two adjacent printing tracks on two layers which is twice the nominal printing resolution defined by the nozzle diameter. The distance between the traces in the grid and between the grid and the edge is also 0.8 mm each, the same as the width of the conductor tracks. The lengths of the traces to the pad of sensor elements 1 - 4 are different, at 285.8 mm, 385.2 mm, 285.8 mm, and 385.2 mm, respectively. The difference is due to the supply lines, which are all routed to the left side of the circuit board housing. Sensor elements 1 and 4 (orange sensor elements in Fig. 2) and 2 and 3 (green sensor elements in Fig. 2) are, therefore, connected in series for evaluation with a total line length of 671 mm each for symmetry. The rear sensor elements have two additional conductors to compensate for the supply lines that pass through the front sensor elements. The sensor elements are connected to a Wheatstone half-bridge circuit on a circuit board by contacting the individual pads of the tracks. This was done with self-adhesive copper foil, silver ink, and solder—for details see Sections 3.6.2 and 3.6.3.

3.4. Analytical approach

An analytical approach with the following simplifications allows an approximate description of the sensor behavior:

- Ideal parallel deformation of the gripping surface using a fixed clamp and a vertical parallel displacement.
- Consider only one of the 1.6 mm thick bending beams for the mechanical calculation.
- Ignore the total moment of inertia of the area with respect to the center axis of the spring body / base body.
- Ignore Poisson's ratio in the mechanical calculation.
- Use the mechanical properties of PETG for both materials due to the small volume fraction of the sensor material.

The calculation of the sensor behavior is based on Hangst et al. [18]. The extension considers the leads' length to the individual sensor elements. While the cross-sections of the connecting wires are larger for standard strain gauges than the conductor tracks in the measuring grid, for this design, the cross-sections of the supply wires and the individual conductor tracks in the measuring grid are the same. This means that the contribution of the length of the leads to the magnitude of the sensor output signal is more significant and cannot be neglected. We performed the calculation of the sensor behavior in two steps. In the first step, the effective change in the length of all sensor elements is determined by a mechanical calculation. Fig. 3 shows the simplified model based on the two bending beams from Fig. 2 with the corresponding sensor elements. Based on the symmetry and context of

$$l_{M_{12}} = l_{M_{34}} = l_{M_{56}} = l_{M_{78}} \quad (1)$$

and

$$\Delta l_{M_{12}} = -\Delta l_{M_{34}} = -\Delta l_{M_{56}} = \Delta l_{M_{78}}, \quad (2)$$

the change in length is the same for all sensor elements. Therefore, it is sufficient to calculate the mean strain in the measuring grid area of

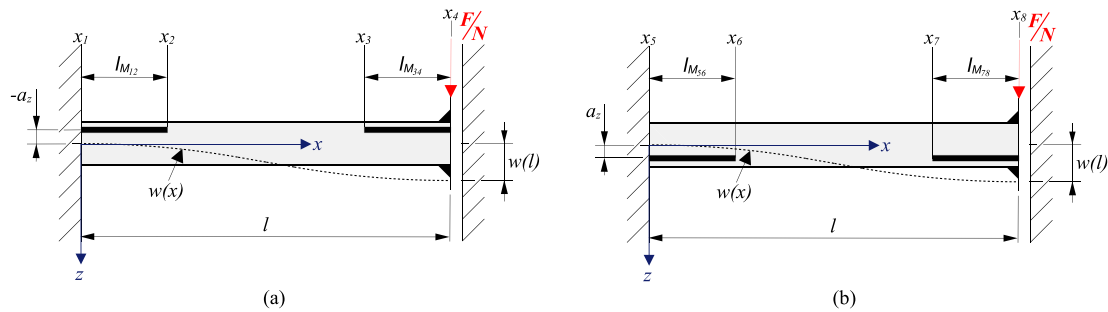


Fig. 3. Sketches of the simplified sensor model of the gripper jaw for the analytical approach. (a) Sensor elements on the upper layers of a beam, (b) sensor elements on the lower layers of a beam.

one sensor element of a beam (Fig. 3(a), top left). In the second step, the differential voltage U_D is calculated from the bridge voltage, the k -factor, and the changes in length of the tracks of all sensor elements with the corresponding initial lengths. In our case, the k -factor for rectangular cross-sections with the edge lengths a and b and the specific electrical resistance ζ , defined by

$$k = 1 - \frac{\Delta a}{\frac{a}{l}} - \frac{\Delta b}{\frac{b}{l}} + \frac{\Delta \zeta}{\frac{\zeta}{l}} = 1 + 2\mu + \eta, \tag{3}$$

must first be determined from the measurement results. The first two terms, $1+2\mu$, where μ is the Poisson's ratio, depend only on the geometric deformation of the material. The third term, η , describes the material-dependent piezoresistive effect. The change in electrical resistance in metals is mainly due to the geometry factor. For semiconductors, the material-dependent piezoresistive effect dominates [31]. The k -factor is always specified for standard strain gauges, approximately 2. The user has to evaluate conductive materials due to the lack of manufacturer specifications.

The fourth-order differential equation, according to the beam theory of Euler-Bernoulli, is utilized as the basis for the mechanical calculation of the bending line w

$$EIw^{IV} = q_0. \tag{4}$$

The Young's modulus E , together with the moment of inertia I , equals bending stiffness, and q_0 is the dead weight of a beam. Since the dead weight of a beam is many times smaller than the applied force F , this term is neglected and set to zero. The bending moment

$$M(x) = \frac{F}{N} \left(x - \frac{l}{2} \right) \tag{5}$$

is obtained by multiple integrations of (4) with appropriate boundary conditions. The total force F applied to the gripper jaw is evenly distributed over the number of beams N . Integrating (5) over the limits x_1 and x_2 divided by their length l_{M12} gives the mean bending moment

$$\bar{M}(l_{M12}) = \frac{1}{l_{M12}} \int_{x_1}^{x_2} M(x) dx. \tag{6}$$

The mechanical strain ϵ_{12} is then obtained by applying the Euler-Bernoulli beam theory together with Hooke's law. The axial strain at the sensor layer is proportional to the local curvature $-w''$, resulting in

$$\epsilon = -w''(x) a_z = \frac{M(x)}{EI} \cdot a_z, \tag{7}$$

where a_z is the signed distance from the neutral axis to the sensor layer. Consequently, the strain ϵ_{12} for the sensor segment is expressed as

$$\epsilon_{12} = \frac{\bar{M}(l_{M12})}{EI} \cdot a_z. \tag{8}$$

Due to the applied coordinate system and the sensor element position (Fig. 3(a), top left), a_z is negative. After calculating the strain ϵ_{12} , the

Table 1
Mechanical and electrical properties of the applied materials.

Parameter	PETG	PLA-C
Yield strength	46 MPa	> PETG
Young's modulus	1930 MPa	3000 MPa
Poisson's ratio	0.42	≈ PETG
Density	1,270 kg·m ⁻³	1,240 kg·m ⁻³
Specific resistance	N/A	10.04 Ω·cm
k -factor	N/A	3.8

effective change in length of the tracks of all sensor elements can be determined by

$$|\Delta l_{ges}| = 4 \cdot l_{M12} \cdot n_w \cdot \epsilon_{12}, \tag{9}$$

where 4 denotes the total number of sensor elements in the jaw, l_{M12} is the measuring length of the measuring grid area of one sensor element, and n_w is the number of tracks per sensor element. After the mechanical characterization, the differential voltage U_D of a Wheatstone half-bridge can be expressed by

$$U_D = \frac{1}{2} U_0 k \left(\frac{|\Delta l_{ges}|}{l_{ges}} \right), \tag{10}$$

where U_0 is the bridge voltage, k is the k -factor, and l_{ges} is the total length of the conductor tracks of all sensor elements, including the supply lines.

3.5. Simulation

The simulation of the sensor behavior is based on the Finite Element Method (FEM) using a linear elastic model and a stationary study with COMSOL 6.3. The material parameters are listed in Table 1. Experimental tests determined the properties of PETG according to DIN EN ISO 527-1. The print directions of the samples corresponded to the print directions of the gripper jaw. Since PETG is an insulating material, the values for electric resistivity and k -factor are neglected. For the conductive PLA-C, the mechanical properties were taken from the literature [29,38]. Due to the low volume fraction of the conductive material, a guideline value is sufficient. In contrast, the resistivity and k -factor have a more significant influence on the behavior of the sensor. They were determined by our tests (see Section 4.1) in combination with the simulation. The manufacturer specifies the resistivity, but it depends on the material batch and printing parameters. The calculations were based on the assumption of isotropic and homogeneous materials for simplicity.

The computation of the sensor behavior is based on a unidirectional coupled simulation between the mechanical and electrical parts. The differential voltage U_D is calculated directly from the applied force F via the resulting deformation of the spring body and the resulting changes in the length of the sensor elements. All simulations were performed using a physics-controlled mesh. A mesh convergence study with adaptive refinement confirmed the numerical accuracy of the results. The calculated

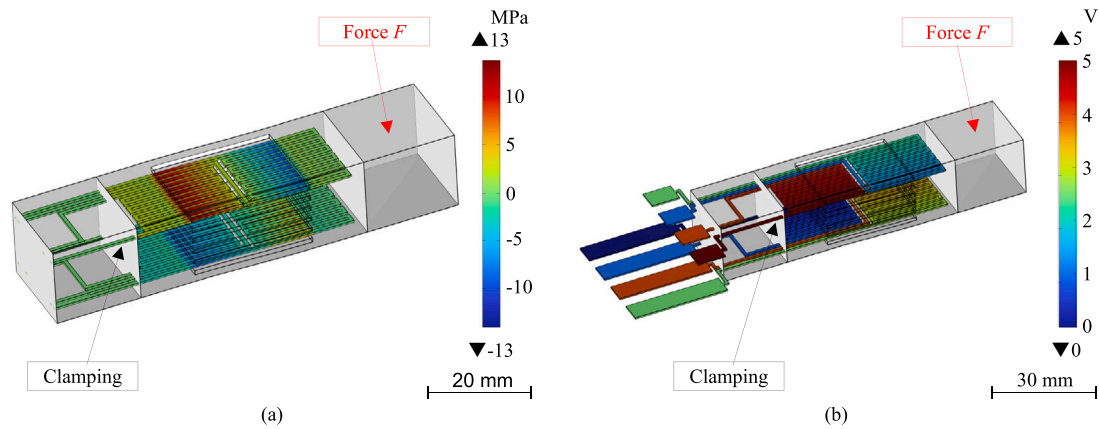


Fig. 4. Simulation results for the gripper jaw under a force of $F = 40$ N. (a) Normal stress distribution in the sensor elements, (b) electrical voltage drop across the sensor elements.

differential voltages varied by less than 0.2 % between successive refinements, indicating convergence and the negligible influence of the mesh on the results. The force F was used in 10 steps from 0 N to 40 N. The maximum force F was also taken from Hangst et al. [18] and is based on the yield strength of PETG, which includes a safety factor of 2.3. The evaluation is performed using a Wheatstone half-bridge circuit for reasons of symmetry. A full-bridge circuit would result in a bridge detuning due to fabrication-related differences in the length of the conductor tracks of the individual sensor elements. Fig. 4(a) shows the mechanical stresses in the gripper jaw's sensor elements at the maximum force F of 40 N, and Fig. 4(b) depicts the resulting electrical voltage drop. The results of the differential voltage U_D are shown together with the measurement results in Section 4.2.2.

3.6. Fabrication process

The gripper jaw was fabricated in three steps: 3D printing, connecting the sensor elements, and integrating the bridge circuit. While step 1 is mainly automated, steps 2 and 3 require manual work.

3.6.1. 3D printing

The gripper jaw was fabricated using fused layer manufacturing (FLM), also known as fused filament fabrication (FFF) or fused deposition modeling (FDM). In this process, molten thermoplastic is sequentially applied through one or more nozzles onto an unheated or heated build platform [24,36,41]. The principle of the additive manufacturing process of the gripper jaw is illustrated in Fig. 5. The print orientation, according to Hangst et al. [18], was retained. The reasons for this are the parallel orientation of the layered structure to the load case in the component and the printing of the sensor elements in one plane. This has the advantage that the conductor tracks can be applied continuously from the beginning to the end without being deposited, thus achieving the best possible conductivity [24,25]. Another advantage is that there are fewer material changes, which makes production more efficient. For the bridges, 1 mm thick object slides were used as a new printing surface for each new beam. This prevents the bridges from sagging and improves the adhesion of the lower layers. It also eliminates the need for separate support material. The carriers can be manually removed after printing. The part has a layer height of 0.2 mm with a line pattern of 45° and a fill density of 100 %. The printing process was interrupted at 2.6 mm, 5.2 mm, 7.8 mm, 10.4 mm, 13 mm, and 15.6 mm to insert the object slides. Other print interruptions occurred at 3 mm, 3.2 mm, 14.2 mm, and 14.4 mm for a manual material change to realize the sensor elements. A printing temperature of 230 °C, as uniform as possible according to Andria et al. [26], was set for both materials to avoid adhesion problems. This corresponds to the maximum printing temperature of the conductive

PLA-C. The default Prusa Slicer setting of 90 °C for PETG was used for the printing bed temperature.

Minor variations in filament feed, layer height, and the geometry of the gripper jaw and conductor tracks can occur during the FLM process. Local fluctuations in material flow, accumulation at the nozzle, or limited repeatability of the printer axes can cause changes in the mechanical properties of the gripper jaw and the sensor elements as well as in the electrical properties of the conductor tracks. Deviations from the exact layer position of the conductor tracks can also affect the measured strain. In addition, the formation and distribution of conductive structures within the polymer matrix can lead to non-reproducible resistance values. As a result, more or less conductive particles are interconnected to different degrees. These variations in resistance values require compensation in practice using external resistors (see Section 4.1.2). This challenge is well known from the literature [22,25,26,33]. Further contributions may also arise from the electrical contact resistance (see Section 3.6.2). Thus, the printing parameters, the matrix material, and the electrical contact resistances all influence the electrical resistance and reproducibility of the sensor elements, while the surrounding 3D-printed structure affects the reproducibility of the sensor signal under mechanical load.

3.6.2. Contacting the sensor elements

In the literature, contacting conductive polymers with interconnect wires is treated differently. Generally, a distinction is made between the use of silver inks / pastes / adhesives [20,24,30,32,39,41], screwing [6], soldering [25,33], welding [26], or melting wires into contact pads [29]. The importance of the contact lies mainly in the resulting electric contact resistance. This should be as low as possible as it directly relates to the sensor's output signal. The higher the resistance, the lower the differential voltage. We used the most common method of applying silver ink in combination with copper pads to keep the contact resistance as low as possible. The first step is to glue the copper pads next to the printed polymer pads in 0.2 mm deep recesses. After soldering the circuit board connecting wires to the copper pads, the copper and polymer pads are coated with conductive silver ink. A final coat of epoxy adhesive is applied to protect the contact surfaces from external influences after the ink has cured. All the fabrication steps for contacting the sensor elements are illustrated in Fig. 6.

3.6.3. Bridge circuit

A circuit board was designed to evaluate the sensor elements using a Wheatstone half-bridge. The board is designed to combine two sensor elements (1 and 4, 2 and 3) into one sensor element each and complete the bridge circuit with two additional parallel passive resistors of 120 Ω each. The circuit board is embedded near the copper pads and sealed

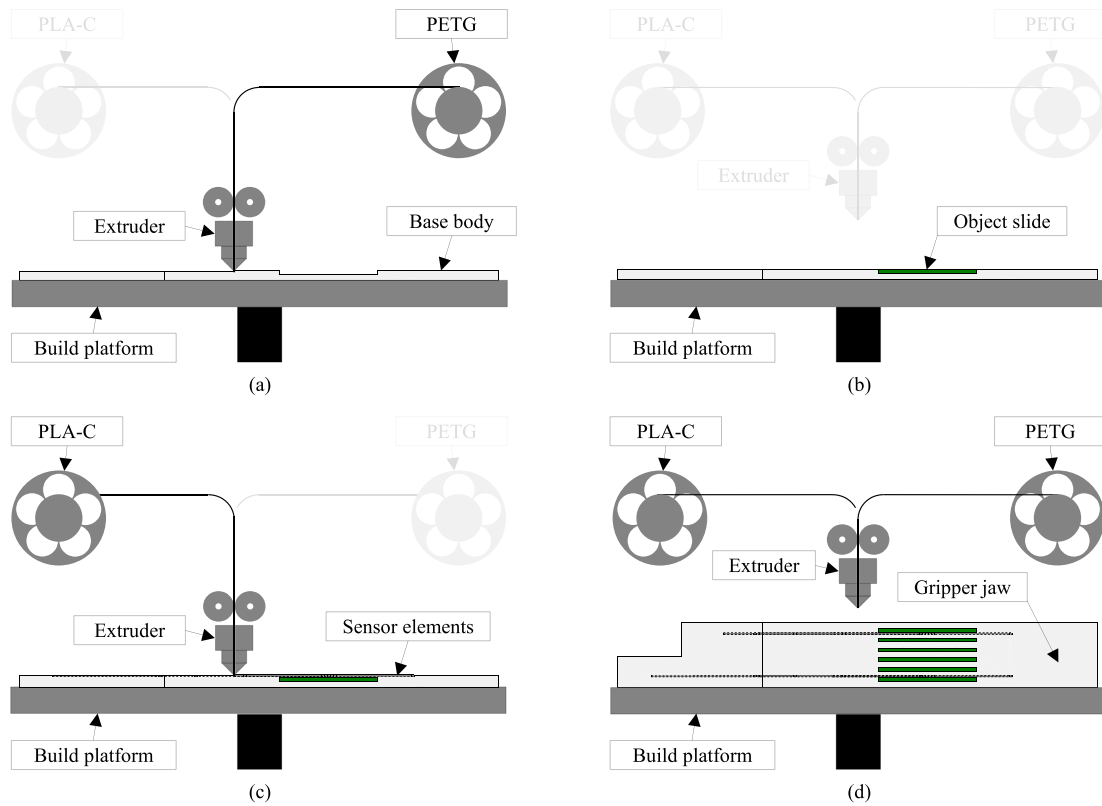


Fig. 5. Schematic representation of the fabrication steps of the gripper jaw. (a) 3D printing of the base body, (b) manual insertion of the object slides, (c) 3D printing of the sensor elements, and (d) fully 3D-printed gripper jaw after several repetitions of the previous process steps, including the object slides for subsequent removal.

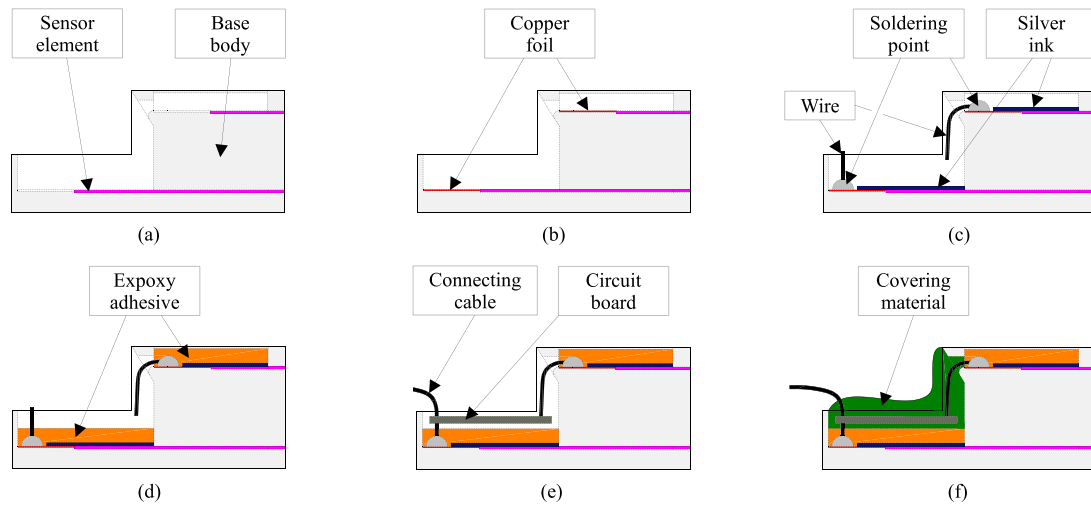


Fig. 6. Schematic representation of the manual fabrication steps for establishing the electrical contact between the sensor elements and the embedded circuit board. (a) Base body with integrated sensor elements, (b) application of the copper foils, (c) soldering of wires to the copper foils and electrical connection of the copper foils with the sensor elements using silver ink, (d) protection of the soldering points and contact areas by applying an epoxy adhesive, (e) placement of the circuit board with the Wheatstone half-bridge followed by soldering to the wires from the copper foils, and (f) application of a covering material to protect the electronics from external influences.

with a covering material to protect it from the environment (see Fig. 6). The fabricated gripper jaw is shown in Fig. 7.

3.7. Measurement setup

This contribution required several measurement setups to characterize the sensor material (PLA-C) and validate the gripper jaw.

3.7.1. Sensor material characterization

The characterization of the sensor material is divided into three steps: determining the specific electric resistance ρ_r , calculating the resistance deviation $R_{i,rel}$ of the individual sensor elements from the adjusted nominal values $R_{i,a}$, and deriving the k -factor. First, the resistivity of the sensor material is measured by taking the output resistance of each of

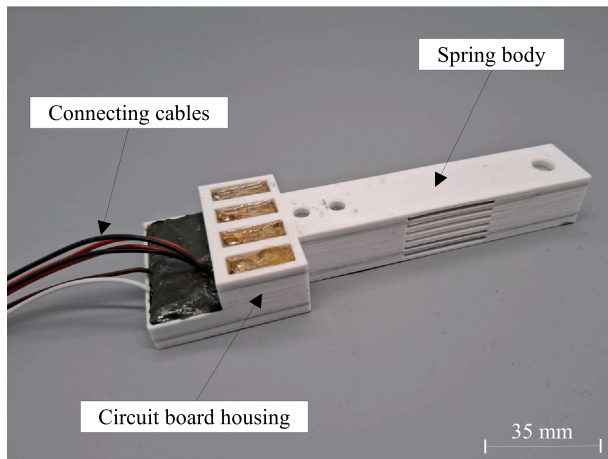


Fig. 7. Fabricated gripper jaw including contacted sensor elements, integrated measuring bridge and connecting cables.

the four sensor elements. For a statistically significant result, 100 measurements were taken with an LCR meter (ST2829C, Sourcetronic), and the mean values, \overline{R}_{r_i} , were calculated. The theoretical resistance values R_{t_i} were determined using simulation, assuming a theoretical resistivity ρ_t of 30 Ω ·cm according to the manufacturer’s specifications. The correction factor K between the theoretical values R_{t_i} and the measurements \overline{R}_{r_i} was set equal to

$$K = -\frac{R_{t_i}}{\Delta R_i - \overline{R}_{r_i}} \quad (11)$$

with

$$\sum_{i=1}^s \Delta R_i = 0, \quad (12)$$

where R_i denotes the difference between the measurements \overline{R}_{r_i} and the adjusted theoretical (nominal) values $R_{t_{a_i}}$. The resistance deviations of the measurements with respect to the adjusted nominal values can be determined by

$$R_{i_{rel}} = \frac{R_{t_{a_i}}}{\overline{R}_{r_i}} - 100 \% \quad (13)$$

with

$$R_{t_{a_i}} = \frac{R_{t_i}}{K}, \quad (14)$$

while the real specific electric resistance can be calculated using

$$\rho_r = \frac{\rho_t}{K}. \quad (15)$$

The k -factor was determined from the measured values in combination with the simulation results.

3.7.2. Gripper jaw validation

The sensitive behavior of the gripper jaw was characterized analogously to Hangst et al. [18] to enable a direct comparison. The basis was DIN EN ISO 376, excluding the measurement of the reversal error. Equations for calculating the characteristic values can be found in Hangst et al. [18]. The experimental setup consists of two parts. Fig. 8 shows the general setup for determining the zero-point deviation, the characteristic value deviation, the linearity behavior, and the repeatability. The extended setup is used for investigating the viscoelastic

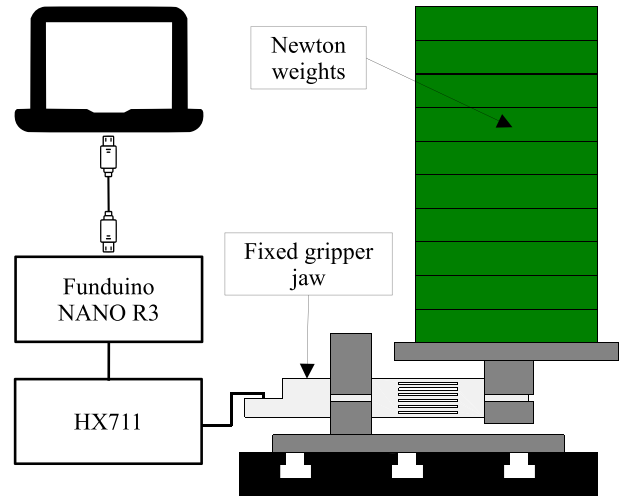


Fig. 8. General measurement setup to determine zero-point deviation, characteristic value deviation, linearity behavior, and repeatability under manual force application with Newtonian weights (adapted from Hangst et al. [18]).

behavior. Both setups are based on the same basic structure and differ only in how the force is applied. In the general setup, the Newton-calibrated weights of 4 N each were applied manually, but in the extended setup, the maximum weight of 40 N was applied automatically by a robot at a speed of 10 mm/s. The zero-point deviation, characteristic value deviation, linearity behavior, and repeatability measurements are performed after reaching the steady state. 100 measurements per step are recorded and evaluated as the mean to obtain statistically significant results. Continuous measurements record the entire time course from applying the force to the steady state to determine the viscoelastic behavior. The sensor signal is evaluated by a Wheatstone half-bridge circuit for symmetry reasons (see Section 3.3). The differential voltage was assessed with a gain factor of 128 and a bridge voltage of 5 V by a 24-bit A/D converter (HX711) in combination with a microcontroller (Funduino NANO R3). The serial data were transferred directly between the Funduino and the PC via a serial interface and stored in a CSV file. The subsequent evaluation was done using MATLAB.

3.8. Arrangements

The gripper jaw was subjected to a warm-up phase of 30 min under excitation voltage. This was followed by a preload phase in which the gripper jaw was loaded and unloaded three times for 60 s with a maximum force of 40 N each time. If several series of measurements were performed immediately after each other, the time between the series of measurements was 3 min. In this case, the warm-up and preload phases were not repeated. All measurements were performed at room temperature under laboratory conditions.

4. Results and discussion

In this section, we present and discuss the measurement results. The measurement results are divided into the sensor material’s electrical characterization and the gripper jaw’s sensitive behavior.

4.1. Sensor material characterization

The electrical material characterization of the sensor material is crucial for the accuracy of the analytical and numerical analysis and for adjusting the measuring bridge.

4.1.1. Specific resistance

The determination of the specific electric resistance ρ_r of the sensor material resulted in a value of 10.04 Ω ·cm with a correction factor K of

Table 2

Resistance values of the individual sensor elements and their deviation from the nominal value.

Sensor element	Measured resistance values	Deviation from nominal value
1	88.711 kΩ	-2.20 %
2	111.948 kΩ	4.76 %
3	92.812 kΩ	-4.59 %
4	118.181 kΩ	0.75 %
1 + 4	206.892 kΩ	-0.52 %
2 + 3	204.760 kΩ	0.52 %

2.9873. The individual resistance values of the sensor elements are listed in Table 2. The deviations by a factor of about three from the manufacturer's specifications can be explained by many factors such as contact type, print orientation, number of layers, line width, print temperature, the 3D printer, material batch, homogeneity of conductive particles in the material, general composition of the material, individual conductive paths through the matrix material, etc. (see Stano et al. [33]). The value ρ_r of 10.04 Ω·cm is many times higher than that of metals due to the matrix material and the filler. This is not important for the fabrication of force-sensing elements. Kim et al. [24] and Stano et al. [25] also reported resistance values for their sensor elements in the range of two to three-digit kilohms.

4.1.2. Resistance deviation of the sensor elements

Measurement of the resistance values of the individual sensor elements has shown that the actual resistance values \bar{R}_r differ from the adjusted theoretical resistance values R_{ta_i} by up to 4.76 %. Therefore, it is not possible to fabricate polymer composite sensor elements with defined resistance values. The reasons are the inhomogeneity of the conductive particles in the raw material and their individual rearrangement of the conductive paths by the matrix material, as well as effects from the printer accuracy and electric contact resistance (see Section 3.6). The deviations of all sensor elements 1 - 4 from the adjusted theoretical resistance values R_{ta_i} and the grouping of two sensor elements 1 and 4, 2 and 3 for the measuring bridge are shown in Table 2. Due to the deviations in resistance values despite the symmetry of sensor elements 1 and 4, 2 and 3, the bridge circuit was poorly tuned. A 2.2 kΩ resistor was connected in series with sensor elements 2 and 3 to solve this problem.

4.1.3. Determination of the k -factor

The k -factor was determined to be 3.8. This value is generally higher than standard metal foil strain gauges, which have a value of about 2. The polymer composite material is according to (3) generally more piezoresistive. Compared to Chadda et al. [29] with the same material, the k -factor is significantly lower (from 8.3 to 3.8). This is due to the following reasons: a different batch/year of production, a change in the material composition, an optimized material, different printing parameters such as layer thickness and printing temperature, the formation of different conductive tracks, etc. An indication of the higher k -factor may be the lower resistivity. This is about 1.24 times higher in Chadda et al. [29]. This suggests that our material contains more filler. Melnykowycz et al. [32] reported that the distance between the conductive particles increases under mechanical stress, decreasing the material's conductivity. This means that the conductive polymer chains are less separated from each other under stress, and, therefore, the k -factor is lower.

4.2. Gripper jaw validation

This contribution focuses on the results of the sensitive behavior of the gripper jaw. Comparisons are also made with comparable partially and fully 3D-printed sensors to classify the sensor quality.

4.2.1. Zero-point deviation

The zero-point deviation is the difference between the output signal before and after a full-scale load cycle (FS). The zero offset was

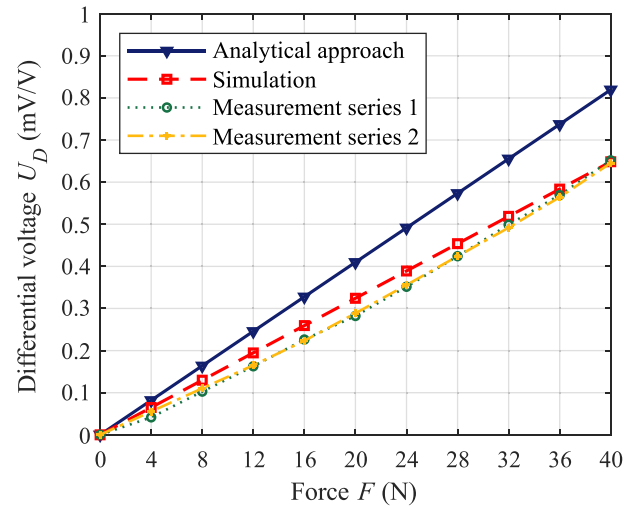


Fig. 9. Results of the analytical approach, the simulation and the two series of measurements for the gripper jaw.

determined based on three load cycles of 60 s each with a maximum relative zero-point deviation $f_{0,max}$ of 1.42 % FS. This corresponds to a value of 0.57 N. Compared to the partially 3D-printed sensor of Hangst et al. [18] with a value of 0.36 % (0.14 N), this is about four times higher. This is due to replacing the constant strain gauge with polymer composite material with conductive and non-conductive particles. The resulting matrix material forms individual conductive paths after processing. When a force is applied, these paths will change, resulting in a change in resistance due to the alteration in the geometry and structure of the material. When the spring body returns after the force is removed, the matrix material may not ultimately return to its original mold, resulting in a zero-point deviation. The zero return will vary depending on how much the conductive path changes. Kim et al. [24] made the same observations on their fully 3D-printed sensor. After 1000 cycles, the offset was approximately 100 %. The most significant offsets were observed in the first few cycles. As the number of cycles increased, the drift became smaller, indicating that the conductor tracks changed less with growing cycles. A saturation towards zero is not visible. The zero-point deviation is the least critical value for gripping applications. The sensor can be reset by software before each load cycle or at specified time intervals.

4.2.2. Characteristic value deviation

The results of the analytical approach, simulation, and measurements are shown in Fig. 9. The mean of the two series of measurements was used to determine the sensitivity deviation. The sensitivity deviation between the simulation and the measurements d_{C_S} is 0 % and is not comparable. The simulation was fitted to the measurements by applying the calculated k -factor of 3.8. The deviation between the analytical approach and the measurements d_{C_A} is -20.86 %. This deviation results from the numerous simplifications explained in Section 3.4. From a plausibility point of view, a negative deviation value indicates the correct direction. This is because the gripper jaw is less stiff when using the same mechanical properties of PETG and conductive PLA-C. As the Young's modulus of the conductive PLA-C increases, the deviation from the measured values decreases.

4.2.3. Linearity behavior

The linearity errors of the two measurement series is shown in Fig. 10(a) and Fig. 10(b). Both series exhibit a similar trend and can be considered reproducible. The maximum value for the linearity deviation d_{lin} of both measurement series through the start and end point is -6.69 % FS and after optimization via linear regression 4.08 % FS. This

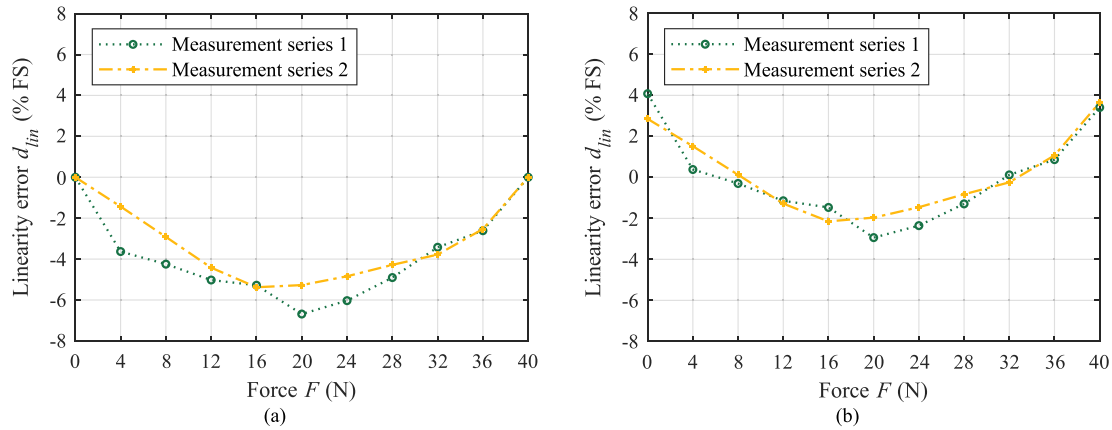


Fig. 10. Linearity behavior of the gripper jaw. (a) Deviation determined using the start- and end-point method, (b) deviation determined using linear regression.

corresponds to a value of 2.28 N and 1.63 N, respectively. Compared to the partially 3D-printed sensor by Hangst et al. [18], with results of -0.21% (-0.084 N) and 0.14% (0.058 N), the values are significantly higher by a factor of about 30. This is also due to the properties of the sensor material (see Section 4.2.1). Compared to the printed strain gauge bonded to a steel plate by Chadda et al. [29], the fully 3D-printed sensors by Stano et al. [33] and Herbst et al. [15], the values are in a similar range. The printed strain gauge by Chadda et al. [29] performs slightly less favorably, with a linearity deviation of about 7 % with linear regression, despite the stiffer steel spring body. This indicates that the sensor material has significantly more influence on the inaccuracies than the base body material. Compared to the fully 3D-printed sensor by Stano et al. [33], the nonlinearities due to the start and end points are lower at 5.17 % and higher at 4.76 % for the linear regression. Herbst et al. [15] report a linearity deviation of 3.6 % via linear regression, which is slightly better than our sensor. Overall, all fully 3D-printed sensors are similar in this respect. Kim et al. [24] also report some nonlinearities. The magnitude of these is not reported in the article.

4.2.4. Repeatability

The repeatability b' indicates the actual force level (RD) deviation at the same installation position. The lowest load of 4 N is 28.5 % RD (0.85 N), representing the maximum value b'_{max} . With increasing force, this value improves and reaches a repeatability of up to 0.89 % RD (0.31 N) at a force of 36 N. The initially high percentage values are due to the more significant influence of small measurement signals in the initial force ranges. The absolute values are all below 1 N. Compared to the partially 3D-printed sensor of Hangst et al. [18], with results of 0.12 % (0.01 N) at a force level of 12 N, the values are many times higher. Fig. 10(a) and Fig. 10(b) show the deviations of the two series of measurements. As described for the zero-point deviation, the traces will be only partially reproducible when the force is applied repeatedly. This effect can be largely reduced by using metal-based sensor elements instead of the conductive polymer, as the inherent crystal structure of the metal provides consistent conductive paths, improving electrical stability and repeatability. Such repeatability tests are rarely performed in the literature. Chadda et al. [29] examined the reproducibility of four measurement series but did not report any values. The accompanying figure suggests a similar behavior compared to our sensor.

4.2.5. Viscoelastic behavior

The viscoelastic behavior was measured under load and unload conditions with a maximum force of 40 N for 6 min each. The results are shown in Fig. 11. The viscoelastic behavior of both materials is evident.

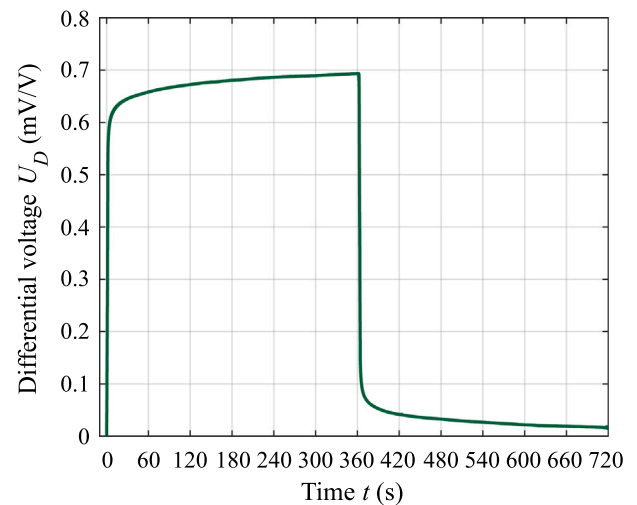


Fig. 11. Viscoelastic behavior of the gripper jaw.

At constant force, the full output signal occurs only over time. As the force is removed, the effect is the same but reversed. The relative creep c between 0 s and 300 s is 22.17 % FS. This corresponds to a value of 8.87 N. The creep deviation c between 30 s and 300 s is significantly lower at 6.25 % FS with a value of 2.5 N. The determination according to the standard from 30 s to 300 s is of no interest for a sensitive gripper jaw since the initial values are needed at the beginning of a gripping process. The values of the viscoelastic properties are the worst characteristic values of the sensor, as in Hangst et al. [18], with results of 2.88 % (1.15 N) and 1.13 % (0.45 N). These are the most significant deviations. Viscoelastic properties are inherent to polymers [24,29]. Similar to repeatability, they could only so far be mitigated through the use of metal-based materials.

4.2.6. Summarized data

All sensor characterization results are summarized in Table 3. Currently, fully 3D-printed sensors do not meet market requirements. Values below 1 % are required [39]. Whether a fully 3D-printed sensor in this form suits a gripping process depends on the application. This sensitive gripper jaw is very suitable for applications with low requirements and for detecting a gripped component. The partially 3D-printed sensor by Hangst et al. [18] should be used for precise tasks with the disadvantages of manual processes and the placement of the strain gauge on the component surface.

Table 3
Summary of the results.

Designation	Abbreviation	Value
Characteristic value deviation analytically	d_{c_A}	-20.86 % FS
Zero-point deviation	f_0	1.42 % FS
Linearity error (start/end point)	d_{lin}	-6.69 % FS
Linearity error (linear regression)	d_{lin}	4.08 % FS
Repeatability	b'_{max}	28.5 % RD
Viscoelastic behavior (creep)	c	22.17 % FS (at 0s) 6.25 % FS (at 30s)

5. Conclusion and outlook

In this contribution, we propose a fully 3D-printed gripper jaw with the beneficial properties of a multiple-bending-beam structure and embedded strain gauges made of a polymer composite material with an extended force range of up to 40 N. Analytical approaches, the finite element method, and experiments were used to investigate the properties of the gripper jaw and the conductive polymer composite material. We have shown that a sensitive gripper jaw can be fabricated functional by 3D printing. Compared to partially 3D-printed sensitive gripper jaws, the properties, especially repeatability and viscoelastic behavior, are less favorable. On the other hand, the sensor elements of the fully 3D-printed gripper jaw are directly integrated into the component, and the fabrication takes place in a single step. In addition, the k -factor is significantly higher than that of standard strain gauges. A disadvantage is the inaccuracy of the electric resistance values during fabrication, which is why compensation resistors are required in the measuring bridge.

In the future, we want to investigate the sensor properties, especially the repeatability and viscoelastic behavior, in more detail and improve them. This will be done by replacing the polymer composite material with sensor elements made of constantan wires. The advantage of replacing the conductive polymer matrix with constantan wires is that the crystal structure of the metal eliminates the variable conductive paths through the sensor elements, improving electrical stability, repeatability, and reproducibility in the fabrication of the sensor elements. The wires also provide reinforcement to the gripper jaw and strengthen the entire spring body, ensuring more consistent deformation under applied load and enhanced elastic recovery after unloading. In addition, the analytical model will be refined by incorporating the actual mechanical properties of both the spring body and the sensor material. This is expected to improve the accuracy of the analytical predictions while maintaining the simplicity of the model. Finally, once the sensitive gripper jaw has been optimized, we want to integrate it into a robotic gripper system to evaluate its performance under realistic industrial conditions. This evaluation will include actuation and control strategies to fully demonstrate the gripping capability in practical applications, as well as to enable comparison with other grippers.

CRedit authorship contribution statement

Nikolai Hangst: Writing – original draft, Visualization, Validation, Software, Project administration, Methodology, Investigation, Formal analysis, Data curation, Conceptualization. **Thomas M. Wendt:** Writing – review & editing, Supervision, Resources, Funding acquisition. **Stefan J. Rupitsch:** Writing – review & editing, Supervision, Resources.

Declaration of generative AI and AI-assisted technologies in the writing process

During the preparation of this work, the authors used DeepL Write in order to improve grammar and clarity of expression. After using this tool, the authors reviewed and edited the content as needed and take full responsibility for the content of the published article.

Funding

This research did not receive any specific grant from funding agencies in the public, commercial, or not-for-profit sectors.

Declaration of competing interest

The authors declare the following financial interests/personal relationships which may be considered as potential competing interests:

Nikolai Hangst has patent #Verfahren zur Herstellung eines Robotererelements, insbesondere eines Greifers, mittels 3D-Druck (Method for Producing a Robot Element in Particular a Gripper, by Means of 3D Printing) issued to Offenburg University of Applied Sciences. Nikolai Hangst has patent Greifelement zum Einsatz in der Robotik und Kobotik (Gripper Element for Use in Robotics and Cobotics) pending to Offenburg University of Applied Sciences. If there are other authors, they declare that they have no known competing financial interests or personal relationships that could have appeared to influence the work reported in this paper.

Acknowledgment

The authors acknowledge support from the Open Access Publication Fund of Offenburg University of Applied Sciences.

Data availability

The data that support the findings of this study are available from the corresponding author upon reasonable request.

References

- [1] L. Kaiser, A. Schlotzhauer, M. Brandstötter, Safety-related risks and opportunities of key design-aspects for industrial human-robot collaboration, In A. Ronzhin, G. Rigoll, R. Meshcheryakov (Eds.), *Lecture Notes in Computer Science, Interactive Collaborative Robotics*, Springer International Publishing, Cham, 2018, pp. 95–104.
- [2] S. Blankemeyer, T. Recker, A. Raatz, Hardwareseitige MRK-Systemgestaltung, In R. Muller, J. Franke, D. Henrich, B. Kuhlenkötter, A. Raatz, A. Verl (Eds.), *Handbuch Mensch-Roboter-Kollaboration*, Hanser, München, 2019, pp. 37–70.
- [3] M.N. Saadatzi, S.K. Das, I.B. Wijayasinghe, D.O. Popa, J.R. Baptist, Precision grasp control with a pneumatic gripper and a novel fingertip force sensor, in: 2018 IEEE 14th International Conference on Automation Science and Engineering (CASE), vol. 82018, Munich, Germany, 2018, pp. 1454–1459.
- [4] L. Kuang, Y. Lou, S. Song, Design and fabrication of a novel force sensor for robot grippers, *IEEE Sens. J.* 18 (4) (2018) 1410–1418, <https://doi.org/10.1109/JSEN.2017.2788015>
- [5] M. Nagel, F. Giese, R. Becker, Flexible gripper design through additive manufacturing, In D. Reinhardt, R. Saunders, J. Burry (Eds.), *Robotic Fabrication in Architecture, Art and Design 2016*, Springer International Publishing, Cham, 2016, pp. 455–459.
- [6] D. Rau, M.R. Burhop, R. Williams, E. Arvanitis, L. Dalloro, Customized robotic grippers with feedback sensors, *WO Patent 2020/041221*, Feb. A1 27, 2020.
- [7] Y. Song, R.A. Boekraad, L. Roussos, A. Kooijman, C.C.L. Wang, J.M.P. Geraedts, 3d printed electronics: Opportunities and challenges from case studies, in: 37th Computers and Information in Engineering Conference, vol. 1, Cleveland, Ohio, USA, 2017.
- [8] L. Stiglmeier, T.M. Wendt, S.J. Rupitsch, 3-d-printed torque sensors: A review, *IEEE Sens. J.* 24 (12) (2024) 18740–18761, <https://doi.org/10.1109/JSEN.2024.3397919>
- [9] S. Junk, N. Hangst, Einsatz von 3D-Multimaterialdruck zur schnellen Herstellung von multifunktionalen Mensch-Roboter-Kollaborations-Greifsystemen, In P. Hoyer, C. Leyens, T. Niendorf, V. Ploshikhin, V. Schulze, G. Wtt (Eds.), *Fachtagung Werkstoffe und Additive Fertigung: 25.-26.04.2018, Tagungsband, Potsdam*, 2018, pp. 115–120.
- [10] N. Hangst, S. Junk, T. Wendt, Design of an additively manufactured customized gripper system for human robot collaboration, in: M. Meboldt, C. Klahn (Eds.), *Industrializing additive manufacturing: Proceedings of AMPA2020*, Cham, Switzerland: Springer, 2021, pp. 415–425.
- [11] R.R. Dehoff, R.F. Lind, L.L. Love, W.H. Peter, B.S. Richardson, *Freeform fluidics*, U.S. Patent 2013/0331949 (Dec. 12, 2013) A1.
- [12] P. Falkowski, B. Wittels, Z. Pilat, M. Smater, Capabilities of the Additive Manufacturing in Rapid Prototyping of the Grippers' Precision Jaws, In R. Szweczyk, C. Zieliński, M. Kaliczyńska (Eds.), *Automation 2019: Progress in Automation, Robotics and Measurement Techniques*, vol. 920, Springer International Publishing, Cham, 2020, pp. 379–387.
- [13] S. Hartomacıoğlu, E. Kaya, B. Eker, S. Dağlı, M. Sarıkaya, Characterization, generative design, and fabrication of a carbon fiber-reinforced industrial robot gripper via additive manufacturing, *J. Mater. Res. Technol.* 33 (2024) 3714–3727, <https://doi.org/10.1016/j.jmrt.2024.10.064>

- [14] G.L. Goh, et al., A 3D printing-enabled artificially innervated smart soft gripper with variable joint stiffness, *Adv. Mater. Technol.* 8 (24) (2023) <https://doi.org/10.1002/admt.202301426>
- [15] F. Herbst, et al., Force sensor for versatile single-step sensor integration in 3D-printed parts, in: 2024 IEEE SENSORS, Kobe, Japan, 2024, pp. 1–4.
- [16] C.-H. Liu, M.-C. Hsu, Y. Chen, W.-T. Chen, T.-L. Chen, A topology-optimized 3D printed compliant finger with flex sensor for adaptive grasping of unknown objects, in: 2019 IEEE/ASME International Conference on Advanced Intelligent Mechatronics (AIM), Hong Kong, China, 72019, 2019, pp. 92–97.
- [17] R. Becker, A. Grzesiak, Robot grip for manipulating articles has at least fixing flange, frame and actuator element made in one piece, *DE Patent 10 (2005) 046 160 C5*, Mar. 22, 2007.
- [18] N. Hangst, T.M. Wendt, T. Seifert, S.J. Rupitsch, Additive manufactured sensitive gripper jaw for extended gripping force ranges in robotics, *IEEE Sens. J.* 25 (16) (2025) 30484–30495, <https://doi.org/10.1109/JSEN.2025.3586583>
- [19] N. Hangst, S. Junk, T. Wendt, Method for producing a robotic element, in particular a gripper, by means of 3D printing, *U.S. Patent 11,491,717 B2*, Aug. 6, 2020.
- [20] B. Shih, et al., Design considerations for 3d printed, soft, multimaterial resistive sensors for soft robotics, *Front. Robot. AI* 6 (2019) 30, <https://doi.org/10.3389/frobt.2019.00030>
- [21] Y. Yang, Y. Chen, Innovative design of embedded pressure and position sensors for soft actuators, *IEEE Robot. Autom. Lett.* 3 (2) (2018) 656–663, <https://doi.org/10.1109/LRA.2017.2779542>
- [22] A. Georgopoulou, B. Vanderborght, F. Clemens, Multi-material 3d printing of thermoplastic elastomers for development of soft robotic structures with integrated sensor elements, in: M. Meboldt, C. Klahn (Eds.), *Industrializing additive manufacturing: Proceedings of AMPA2020*, Cham, Switzerland: Springer, 2021, pp. 67–81.
- [23] J.F. Christ, N. Aliheidari, P. Pötschke, A. Ameli, Bidirectional and stretchable piezoresistive sensors enabled by multimaterial 3d printing of carbon nanotube/thermoplastic polyurethane nanocomposites, *Polymers* 11 (1) (2018) <https://doi.org/10.3390/polym11010011>
- [24] K. Kim, J. Park, J. Suh, M. Kim, Y. Jeong, I. Park, 3d printing of multi-axial force sensors using carbon nanotube (CNT)/thermoplastic polyurethane (TPU) filaments, *Sens. Actuators A Phys.* 263 (2017) 493–500, <https://doi.org/10.1016/j.sna.2017.07.020>
- [25] G. Stano, A. Di Nisio, A.M. Lanzolla, M. Ragolia, G. Percoco, Fused filament fabrication of commercial conductive filaments: experimental study on the process parameters aimed at the minimization, repeatability and thermal characterization of electrical resistance, *Int. J. Adv. Manuf. Technol.* 111, 9–10, pp. (2020) 2971–2986, <https://doi.org/10.1007/s00170-020-06318-2>
- [26] G. Andria, A. Di Nisio, A. Lanzolla, G. Percoco, G. Stano, Design and characterization of innovative 3D printed embedded strain gauges, in: 2019 IEEE 5th International Workshop on Metrology for AeroSpace (MetroAeroSpace), vol. 62019, Torino, Italy, 2019, pp. 54–59.
- [27] Y. Xu, et al., The boom in 3d-printed sensor technology, *Sens.* 17 (5) (2017) <https://doi.org/10.3390/s17051166>
- [28] O. Kanoun, A. Bouhamed, R. Ramalingame, J.R. Bautista-Quijano, D. Rajendran, A. Al-Hamry, Review on conductive polymer/CNTs nanocomposites based flexible and stretchable strain and pressure sensors, *Sens.* 21 (2) (2021) <https://doi.org/10.3390/s21020341>
- [29] R. Chadda, O.B. Dali, B. Latsch, E. Sundaralingam, M. Kupnik, 3d-printed strain gauges based on conductive filament for experimental stress analysis, in: 2023 IEEE SENSORS, vol. 10292023, Vienna, Austria, 2023, pp. 1–4.
- [30] M. Liu, Y. Zhao, Y. Shao, Q. Zhang, C. Liu, 3d printed force sensor with inkjet printed piezoresistive based strain gauge, in: 2018 IEEE SENSORS, vol. 102018, New Delhi, 2018, pp. 1–4.
- [31] H.-R. Tränkle, L. Reindl, *Sensortechnik*, Springer, Berlin, Germany, 2014.
- [32] M. Melnykowycz, B. Koll, D. Scharf, F. Clemens, Comparison of piezoresistive monofilament polymer sensors, *Sens.* 14 (1) (2014) 1278–1294, <https://doi.org/10.3390/s140101278>
- [33] G. Stano, A. Di Nisio, A. Lanzolla, G. Percoco, Additive manufacturing and characterization of a load cell with embedded strain gauges, *Precis. Eng.* 62 (2020) 113–120, <https://doi.org/10.1016/j.precisioneng.2019.11.019>
- [34] D. Espalin, D.W. Muse, E. MacDonald, R.B. Wicker, 3d printing multifunctionality: Structures with electronics, *Int. J. Adv. Manuf. Technol.* 72, 5–8, pp. 2014 963–978, <https://doi.org/10.1007/s00170-014-5717-7>
- [35] J. Qu, Q. Wu, T. Clancy, Q. Fan, X. Wang, X. Liu, 3d-printed strain-gauge micro force sensors, *IEEE Sens. J.* 20 (13) (2020) 6971–6978, <https://doi.org/10.1109/JSEN.2020.2976508>
- [36] J. Qu, Q. Wu, T. Clancy, X. Liu, Design and calibration of 3d-printed micro force sensors, in: 2016 International Conference on Manipulation, Automation and Robotics at Small Scales (MARSS), vol. 72016, Paris, France, 2016, pp. 1–4.
- [37] J.A. Lewis, M.A. Bell, T.A. Busbee, J.E. Minardi, J.E. Minardi II, Printed three-dimensional (3D) functional part and method of making, *U.S. Patent 2016/0198576* (Jul. 7, 2016) A1.
- [38] A. Fischer, D. Achten, M. Launhardt, *Kunststoff-Wissen für die additive Fertigung: Eigenschaften, Verarbeitung und Einsatzgebiete von Thermoplasten*, Hanser, München, 2023.
- [39] K.-Y. Joung, S.-Y. Kim, I. Kang, S.-H. Cho, 3d-printed load cell using nanocarbon composite strain sensor, *Sens.* 21 (11) (2021) <https://doi.org/10.3390/s21113675>
- [40] P. Pan, et al., Robotic stimulation of freely moving drosophila larvae using a 3d-printed micro force sensor, *IEEE Sens. J.* 19 (8) (2019) 3165–3173, <https://doi.org/10.1109/JSEN.2018.2886186>
- [41] S.J. Leigh, R.J. Bradley, C.P. Purssell, D.R. Billson, D.A. Hutchins, A simple, low-cost conductive composite material for 3D printing of electronic sensors, *PLoS One* 7 (11, e49365, 2012) <https://doi.org/10.1371/journal.pone.0049365>

Author biography

Nikolai Hangst received the bachelor's and master's degrees in industrial engineering from the University of Applied Sciences Offenburg, Offenburg, Germany, in 2016 and 2018, respectively. He is currently pursuing the Ph.D. degree with the Department of Microsystems Engineering, University of Freiburg, Freiburg, Germany, with a focus on additive manufactured sensitive gripper jaws. His fields of research include robotics, additive manufacturing, and 3D printed sensors.

Thomas M. Wendt received the Ph.D. degree in microsystems technology from the Faculty of Technology, Albert-Ludwigs-Universität Freiburg, Freiburg im Breisgau, Germany, in 2008. Currently, he holds the position of Professor with the Faculty of Economics, University of Applied Sciences at Offenburg, Offenburg, Germany. He also leads the Work-Life Robotics Institute, University of Applied Sciences at Offenburg. His primary research focuses include measurement technology, robotics, additive manufacturing, and human-machine interaction.

Stefan J. Rupitsch (Member, IEEE) was born in Kitzbühel, Austria, in 1978. He received the Diploma and Ph.D. degrees in mechatronics from Johannes Kepler University Linz, Linz, Austria, in 2004 and 2008, respectively, and the Habilitation degree from the University of Erlangen Nurnberg, Erlangen, Germany, in 2018. In 2004, he was a Junior Researcher with the Linz Center of Mechatronics, Linz. From 2005 to 2008, he was with the Institute for Measurement Technology, Johannes Kepler University Linz. From 2008 to 2020, he was with the Chair of Sensor Technology, University of Erlangen Nurnberg, where he held a Deputy Professorship. Since December 2020, he has been a Full Professor of Electrical Instrumentation and Embedded Systems with the University of Freiburg, Freiburg im Breisgau, Germany. He has authored more than 200 articles in these fields and the book *Piezoelectric Sensors and Actuators: Fundamentals and Applications*. His research interests include piezoelectric transducers, energy harvesting, embedded systems, ultrasonic imaging and therapy, simulation-based material characterization, and noncontact measurements. Dr. Rupitsch was a recipient of the Austrian Society of Measurement and Automation Technology Award for his Ph.D. dissertation in 2009 and the Outstanding Paper Award of the Information Technology Society in 2016. He is an Associate Editor of *IEEE SENSORS JOURNAL* and the *Technisches Messen (TM)* journal. He serves as a Guest Associate Editor for the *JOURNAL OF SENSORS AND SENSOR SYSTEMS (JSSS)*.